PNAS RESEARCH ARTICLE | PHYSIOLOGY

Mechanism of voltage sensing in Ca^{2+}- and voltage-activated K^+ (BK) channels

Willy Carrasquel-Ursulaez[a,1,2], Ignacio Segura[a,2], Ignacio Díaz-Franulic[a,b], Valeria Márquez-Miranda[h], Felipe Echeverría[a], Yenisleidy Lorenzo-Ceballos[a,1], Nicolás Espinoza[a], Maximiliano Rojas[b], Jose Antonio Garate[a,c,d], Eduardo Perozo[e,f], Osvaldo Alvarez[a,g], Fernando D. Gonzalez-Nilo[a,b,3], and Ramón Latorre[a,3]

Edited by Mark Nelson, University of Vermont, Burlington, Vermont; received March 20, 2022; accepted May 10, 2022

In neurosecretion, allosteric communication between voltage sensors and Ca^{2+} binding in BK channels is crucially involved in damping excitatory stimuli. Nevertheless, the voltage-sensing mechanism of BK channels is still under debate. Here, based on gating current measurements, we demonstrate that two arginines in the transmembrane segment S4 (R210 and R213) function as the BK gating charges. Significantly, the energy landscape of the gating particles is electrostatically tuned by a network of salt bridges contained in the voltage sensor domain (VSD). Molecular dynamics simulations and proton transport experiments in the hyperpolarization-activated R210H mutant suggest that the electric field drops off within a narrow septum whose boundaries are defined by the gating charges. Unlike Kv channels, the charge movement in BK appears to be limited to a small displacement of the guanidinium moieties of R210 and R213, without significant movement of the S4.

voltage sensitivity | allosterism | BK channels | potassium channels

Excitable tissues accomplish their signaling functions thanks in part to the interplay of several voltage-sensitive ion channels (1–6). Hence, to understand these processes, it is crucial to establish how voltage-sensitive ion channels sense changes in the electric field across the membrane, an issue that has been a matter of extensive study and intense debate for decades. The most widely accepted mechanism proposes the existence of voltage-sensor domains (VSDs), modules that undergo two or more discrete conformational states in response to changes in the membrane voltage. The simplest model considers two states: active (A), which promotes pore opening, and resting (R), which promotes channel closing. To accomplish its function, VSDs contain voltage-sensitive particles, which move in response to changes in the electric field. This movement triggers the interconversion between the two discrete conformational states. These voltage-sensing particles are typically the guanidine groups of arginine residues within the S4 transmembrane segment, which undergo a combination of rotational, translational, and tilting movement in response to changes in membrane voltage (7–14).

The large-conductance Ca^{2+}- and voltage-activated K^+ (BK) channels have a wide distribution in mammalian tissues (15–18), where they participate in a diversity of physiological processes. Their malfunction is often related to diverse pathological conditions (19, 20). BK channel open probability is independently regulated by membrane depolarization and intracellular Ca^{2+} concentration (21, 22), each stimulus being detected by specialized modules. Like other voltage-sensitive K^+ (Kv) channels, BK is an homotetramer in which each of its α subunits consists of a pore domain (PD; S5-S6 transmembrane segments), a voltage-sensing domain (VSD; S1–S4 transmembrane segments) containing a positively charged S4, and a cytosolic C-terminal regulatory domain, which contains the Ca^{2+}-binding sites (23, 24). Also, like some members of other K^+ channel families (25, 26), the VSD and PD of BK are non–domain swapped (23, 24). BK channels display some distinctive structural and functional features: Despite sharing the selectivity filter sequence with Kv channels, BK unitary conductance and selectivity are exquisitely high (27–30). The BK α subunit has an additional transmembrane segment S0 [therefore, its N terminus faces the extracellular medium (31)], and the voltage sensitivity in BK channels is significantly lower than that of Kv channels, presumably because of their lower number of gating charges (32).

Although thoroughly studied, research into BK VSD and its voltage dependence has faced several technical obstacles. The relatively small gating charge per channel (32) and the large conductance of the BK pore makes isolating of the gating currents from the ionic currents a tough experimental challenge. In addition, because mutations of VSD residues can produce very large shifts in both the gating charge-voltage ($Q(V)$) and the conductance-voltage $G(V)$) relationships (33), it is necessary to use extreme

Significance

BK channel voltage sensitivity is paramount for the physiology of excitable and nonexcitable tissues. Although the structure of the voltage sensor domain and number of charged residues in the S4 of BK is like that of Kv channels, BK voltage dependence is much weaker. Here, using gating current measurements and microsecond molecular simulations, we show that two S4 charges (R210 and R213) are the voltage-sensing particles. These residues undergo a small upward rotameric displacement in a septum devoid of water with only slight movement of S4 during activation. These findings explain the weak voltage dependence in BK and show that the mechanism of voltage sensing in BK channels is altogether different from that of Kv channels.

Author contributions: W.C.-U. and R.L. designed research; W.C.-U., I.S., I.D.-F., V.M.-M., F.E., Y.L.-C., N.E., M.R., and J.A.G. performed research; W.C.-U., I.S., I.D.-F., V.M.-M., E.P., O.A., F.D.G.-N., and R.L. analyzed data; and W.C.-U., I.S., I.D.-F., E.P., O.A., F.D.G.-N., and R.L. wrote the paper.

The authors declare no competing interest.

This article is a PNAS Direct Submission.

[1]Present address: Department of Anesthesiology, Washington University in St. Louis, St. Louis, MO 63110.

[2]W.C.-U. and I.S. contributed equally to this work.

[3]To whom correspondence may be addressed. Email: ramon.latorre@uv.cl; or fernando.gonzalez@unab.cl.

This article contains supporting information online at http://www.pnas.org/lookup/suppl/doi:10.1073/pnas.2204620119/-/DCSupplemental.

Published June 15, 2022.

voltages to accurately measure the voltage dependence of some mutants. Consequently, the identification of BK gating charges has been addressed by using indirect approaches (33, 34). The combination of electrophysiology measurements and kinetic modeling suggests a decentralized VSD in the BK channel, where four charged residues (D153 and R167 in S2, D186 in S3, and R213 in S4) act as voltage sensor particles (33). A recent report of the atomistic cryo-electron microscopy (cryo-EM) structures of the human BK channel and its homolog in *Aplysia californica* (AcSlo) revealed minor structural differences between the VSD in both the Ca^{2+}-bound (open pore) and the Ca^{2+}-unbound (closed pore) conformations (23, 24, 35). This result can be explained if the conformational changes of the BK VSD upon activation are small compared to those that occur during the activation of other channels, such as HCN channels (12–14).

In this study, we identified voltage-sensing particles in the BK channel by using a direct functional approach, involving gating of current measurements and analysis of the $Q(V)$ curves spanning 800 mV in the voltage axis. Systematic neutralization of the individual charged residues in the VSD (S1–S4) revealed that only the neutralization of two arginines in S4 (R210 and R213) changed the voltage dependence of the $Q(V)$ curves. Neutralization of other VSD charges point to roles in tuning of the half-activation voltage of the VSD and its allosteric coupling with the PD. Molecular dynamics (MD) simulations based on the cryo-EM structures of the human BK channel (35) as templates suggested that R210 and R213 lie in a very narrow septum separating intra- and extracellular water-filled vestibules. This interpretation is consistent with the robust hyperpolarization-activated proton currents generated when R210 is mutated to the protonable amino acid histidine. Overall, our results point to a unique and distinctive mode of activation in BK: In contrast to Kv channels, where positive charges move one by one through a charge transfer center (absent in BK channels) that spans the entire electric field (36, 37), charge movement in BK channels is limited to the small displacement of R210 and R213, which itself constitutes a narrow septum where the electric field drops.

Results

Neutralization of Two S4 Arginines Changes the Voltage Dependency of Voltage Sensor Activation. Charged residues in the VSD (S1–S4) of the BK channel (Fig. 1*A*) were systematically neutralized to evaluate their role in voltage sensing. Gating currents were recorded in the wild-type (wt) and mutant BK channels (Fig. 1*B* and *SI Appendix*, Fig. S1). Gating charges were calculated by integrating the early gating currents elicited by the voltage steps using a previously reported procedure that excludes charge displacements associated with channel opening (21, 38–40) (*SI Appendix, Materials and Methods*). Since the half-activation voltages (V_0) of mutants R207Q and R210Q were largely leftward shifted (Fig. 1*B*), in these cases the charge displaced was calculated by integrating the gating currents after the end of the voltage steps. The apparent number of gating charges per subunit (z_Q) was obtained from a fit of the $Q(V)$ data (Fig. 1*C*) by using a Boltzmann sigmoid function (Eq. **5** in *SI Appendix, Materials and Methods*). The z_Q values are summarized in Fig. 1*D* and *SI Appendix*, Table S1. Only two charge neutralizing mutations, R210Q and R213Q, resulted in a significant reduction of z_Q (Fig. 1*D* and *SI Appendix*, Table S1), as seen from the lower slope of the $Q(V)$ curves at V_0 (Fig. 1*C*). These mutations also led to the largest shifts of V_0 relative to the wt (Fig. 1*C* and *SI Appendix*, Table S1), with V_0 values of -342 ± 11 mV (R210Q) and 394 ± 1 mV (R213Q). These results suggest that this pair of charged residues plays a major role in the voltage sensing and tuning of the free energy necessary to open the channel. Thus, we propose that R210 and R213 are the only voltage-sensing residues in the BK channel VSD.

Since the fast component of the gating current (I_g) follows single-exponential kinetics, the BK's VSD activation can be described by using a simple two-state model consisting of a resting (R) state and an active (A) state. The voltage-dependent equilibrium constant $J(V)$ that defines the A–R equilibrium is

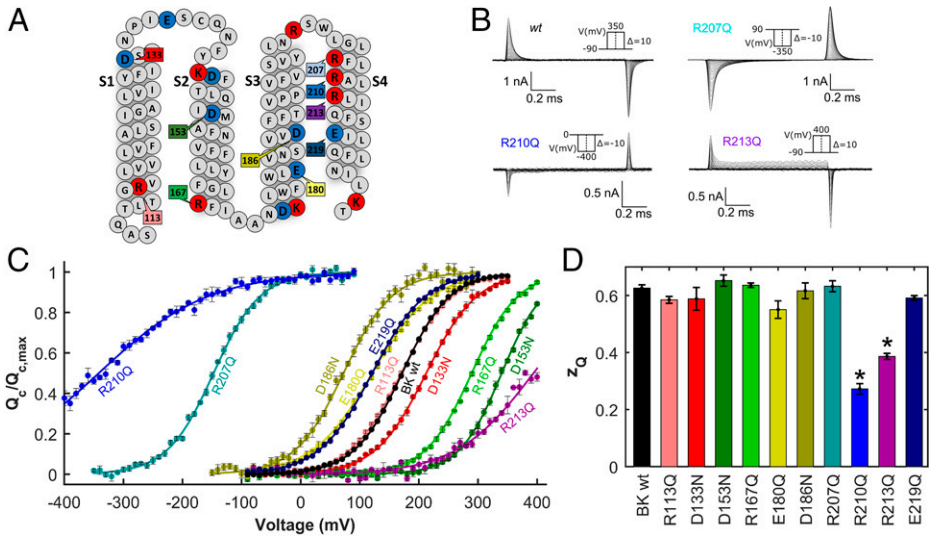

Fig. 1. Gating charge displacement for neutralization mutants in the VSD of the human BK channel. (*A*) Primary amino acid sequence of the VSD (S1 to S4). Positively charged residues are colored blue, and negatively charged residues are colored red. Residues that were neutralized are highlighted with their number in the primary sequence. Letters represent symbols for amino acids. (*B*) Representative records of gating current of BK wt and neutralization mutants R207Q, R210Q, and R213Q. (*C*) Gating charge versus voltage ($Q(V)$) curves at zero internal calcium. Except for R210Q and R207Q, $Q(V)$ curves were constructed from the integration of the ON gating currents recorded after a depolarization from −90 mV to a voltage ranging between 300 mV and 400 mV depending on the mutant tested, in 10 mV steps. For R210Q and R207Q, the holding potential was +90 mV, and gating currents were recorded during the OFF current in the voltage range of 90 to −400 (R210Q) or −350 mV (R207Q) in 10 mV steps. (*D*) Half-activation voltage (V_0) and the apparent number of gating charges (z_Q) for the BK wt and for mutants bearing neutralizing substitutions were obtained from the fitting of the $Q(V)$ data to Eq. 8 in *SI Appendix, Materials and Methods*. (*SI Appendix*, Table 1 and Fig. S1 provides examples of raw gating currents). *$P < 0.01$. Error bars in *C* and *D* = SD.

$$J(V) = \frac{A}{R} = e^{\frac{z_J F}{RT}(V - V_0)} \quad [1]$$

where z_J (equivalent to z_Q) is the charge associated with voltage sensor activation. From Eq. 1, it follows that the difference in free energy (ΔG^0)—at 0 mV—between both states is

$$\Delta G^0 = z_J F V_0 \quad [2]$$

The difference in ΔG^0 for a particular mutant (ΔG^0_{mut}) compared with that for the wt (ΔG^0_{WT}) is defined as

$$\Delta(\Delta G^0) = \Delta G^0_{mut} - \Delta G^0_{WT} \quad [3]$$

Except for R210 and R213, whose singular effects will be analyzed in detail below, the rest of the neutralization mutants did not change the voltage dependence of $Q(V)$. We classified these mutations into two groups: those shifting the $Q(V)$ curves to more depolarized potentials along the voltage axis (D133, R167, and D153), biasing the $A - R$ reaction toward the resting state ($\delta(\Delta G^0) > 0$) (Fig. 1*C* and *SI Appendix*, Table S1), and those shifting the $Q(V)$ curves toward more hyperpolarized potentials (R207, D186, E180, and E219), stabilizing the active state ($\delta(\Delta G^0) < 0$) (Fig. 1*C* and *SI Appendix*, Table S1). For these mutants, charge neutralization did not lead to changes in z_Q, implying that none of them determines the voltage sensitivity of the VSD. Consequently, despite residues D153, R167, and D186 being crucial in determining the V_0, we no longer consider them to be potential voltage-sensing residues, as previously proposed (33).

A Dry Zone Defines the VSD Septum. To explore VSD dynamics at the molecular level, we performed full atomistic MD simulations of the 3.5-Å closed h*Slo*1 cryo-EM structure (35) embedded in a phospholipid bilayer and explicit solvent (Fig. 2*A*). In the absence of a charge transfer region, as found in other Kv channels (36), we first determined where the transmembrane electrical potential is most likely to fall by investigating the degree of hydration of the VSD. In Fig. 2*B*, dark blue, the extent of hydration of one BK channel VSD (S1–S4) shows that R210 is in a region essentially devoid of water and that R213 lies at an interface between an internal aqueous vestibule and a zone where the water density decreases abruptly. This observation is quantitated in Fig. 2*C*, wherein the hydration profiles of the four VSDs (residues 93 to 326) are presented in the form of average densities (in time and for the four VSDs) along the axial dimension (i.e., z axis) and within a cylinder centered around the R210-R213 region and on two planes that cross the R210-R213 positions (Fig. 2*D*). Overall, the water density around R210-R213, a region that comprises ~12 Å, is significantly reduced compared with bulk conditions, with values close to zero at the R210 position. Thus, the dry zone of the VSD defines the region of the channel likely to encompass most of the drop in the transmembrane electric field.

A Histidine at Position 210 Promotes Voltage-Dependent Proton Transport. Starace and Bezanilla (41, 42) showed that replacing some of the voltage-sensing arginines in the S4 of Shaker with histidines (pKa = 6.2 for its side chain) transformed their VSD into either a proton channel or a proton

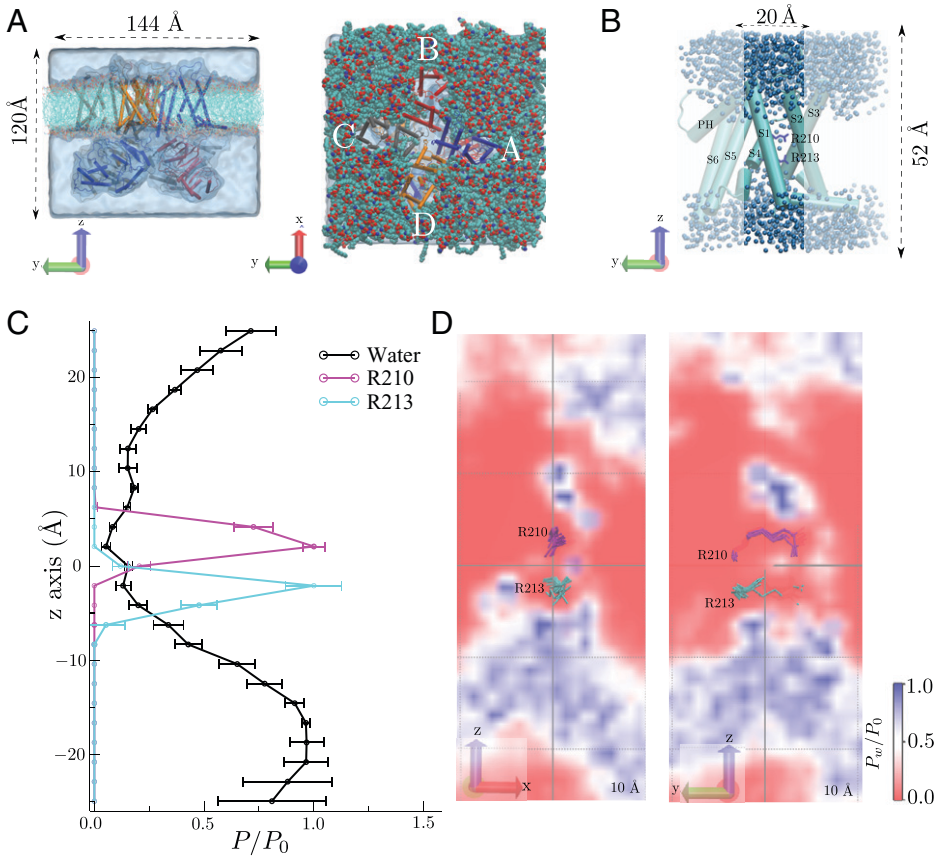

Fig. 2. Molecular simulations shows a VSD dry zone around the BK channel gating charges. (*A*) Side (*Left*) and top (*Right*) views of the simulated system, where the h-BK channel (PDB ID: 6V35), lipids, and water are presented in cartoon, transparent surface, and cyan representations, respectively. (*B*) Representative snapshot of VSD monomer. Unshaded regions depict the region employed for density calculations shown in *C*. (*C*) Relative densities of water, R210, and R213 within a 10-Å radius cylinder along z −25 Å < z < 25 Å. Error bars represent the time average over the four chains. (*D*) Water density profile in a plane crossing the R210-R213 pair (shown in magenta and cyan licorice representation, respectively) and centered at the origin.

transporter. These results are a clear demonstration that the residues must be displaced in the electric field in a very narrow region, namely the charge transfer center (36). The gating characteristics of the histidine mutants depend on the mechanism by which they transport protons. A transporter-like behavior predicts that under a pH gradient, the histidine-mediated proton current should reach a maximum at the voltage of half-activation (41). On the other hand, the formation of a proton pore predicts the existence of a very narrow barrier that separates water and protons and focuses the electric field (42). The low values of z_Q (Fig. 1 *C* and *D*) strongly suggest that R210 and R213 do not move through the entire electric field, which is also consistent with the existence of a broad (>10 Å) septum that defines the region where the membrane electric field is focused. We therefore reasoned that a histidine placed in position 210 should reduce the z_Q at neutral or basic pH and that the z_Q value of the wt should be recovered when the $Q(V)$ is determined from the OFF-gating currents at pH values low enough to confer a positive charge to the arginine side chain. As expected, the z_Q value (0.28 ± 0.02) of the R210H mutant at symmetrical pH 7.4 (Fig. 3 *A* and *B* and *SI Appendix*, Table S1) is nearly identical to that of the R210Q mutant. However, we found that when the external pH was reduced to 5.1, inward ionic currents were developed as long as the VSD resting state became populated at very negative voltage values (Fig. 3*C*). These proton currents had all the characteristics of those of an inward rectifier channel (Fig. 3*D*). These results suggest that i) in the resting state of the VSD, histidine 210 lies at the interface of the septum and the internal crevasse of the VSD and ii) despite having a low water density (0.2 compared with the bulk; Fig. 2*C*), this septum has, in a pH gradient, enough protons to generate an inward current aided by the thermal fluctuations driving the H210 movement between the septum and the intracellular (high pH) solution.

The Membrane Electric Field Is Focused on the R210–R213 Pair. The electrostatic potential (Φ) for a VSD (from now chain A; Fig. 4*A*) on a R210-R213 focused plane (electrostatic potential maps of the other three VSDs, chains B to D, are shown in *SI Appendix*, Fig. S2) was computed for the most representative structure of the 0.5-μs MD ensemble (Fig. 4*A*). The average Φ over the four monomers along the *z* axis within a cylinder centered on the R210-R213 geometric center is shown in Fig. 4*B*. Altogether, positive Φ values encompass an ∼10-Å region, which colocalizes with the VSD dehydration zone and therefore with higher densities of both arginines during the simulation, particularly R210 (Fig. 2*C*). Specific interactions between R210-213 and negative residues were quantified in the form of average distances of the interacting pairs (Fig. 4*C*). R213 exhibits a lower average distance toward D186 than R210, thus contributing to the lower Φ measured at its position. Likewise, R207 presents two interactions with D133 and D153, hence the lack of positive Φ values above the R210-213 region. We also computed the average electrostatic solvation energies of R210 and R213 within the VSD, which yielded values of −161.2 ± 1.4 and −172.6 ± 0.4 kJ/mol, respectively, consistent with the lower hydration, more positive Φ, and reduced specific interactions of R210 with its surroundings.

BK Gating Charges Experience a Small Vertical Movement during Channel Gating. To study the evolution of the gating charge displacement from the resting state (no electric field applied) toward the active state, three MD simulations of the BK channel structure (Protein Data Bank [PDB] ID: 6V35) were done under a 400-mV depolarizing membrane voltage for 3.9 and 2.3 μs (two replicas) (Fig. 5 and *SI Appendix*, Fig. S4). The simulations consistently showed that the R210 guanidine groups underwent a rotameric upward average displacement of around 4.0 ± 1.5 Å along the *z* axis, with the four voltage sensors seemingly behaving in an independent fashion (Fig. 5*A* and *SI Appendix*, Fig. S4 *A* and *B*, *Top*). In the 3.9-μs replica, one of the voltage sensors reacted almost immediately to the application of the electric field (Fig. 5*A*; sensor D, blue trace), whereas the R210 contained in sensor A (black trace) acquired the active configuration only after about 1.5 μs while the other two sensors reached the active state at around 0.5 μs. The

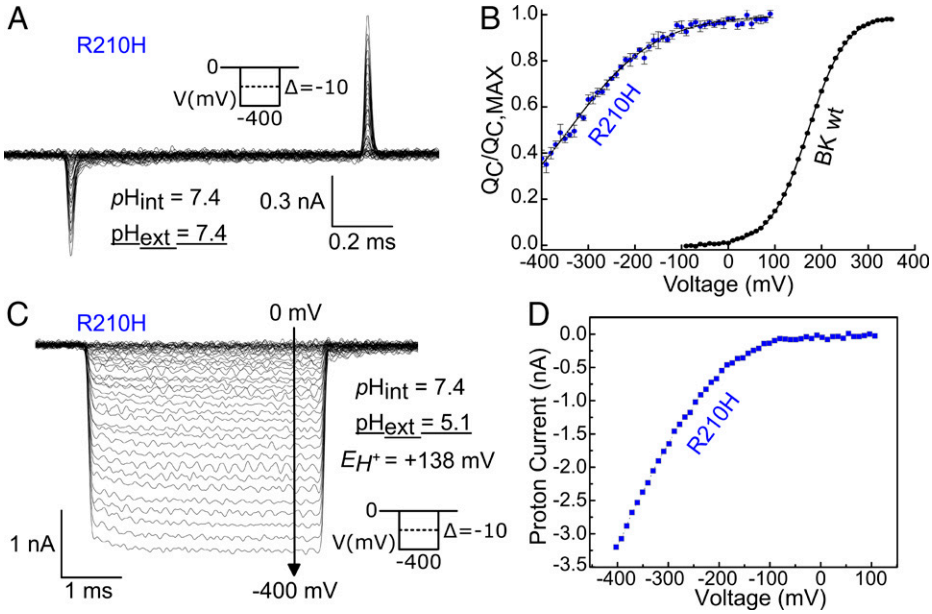

Fig. 3. Hyperpolarization-activated proton pore reveals a distinctive VSD activation mechanism. (*A*) Representative gating current recording for R210H channel under symmetrical pH conditions. (*B*) External acidification protonates the histidine at this position, forming an inward rectifying proton channel. Error bars = SD. (*C*) $Q(V)$ relationship for R210H mutant obtained at symmetrical pH = 7.4. (*D*) Steady-state current versus voltage curve obtained from current records such as those shown to the left.

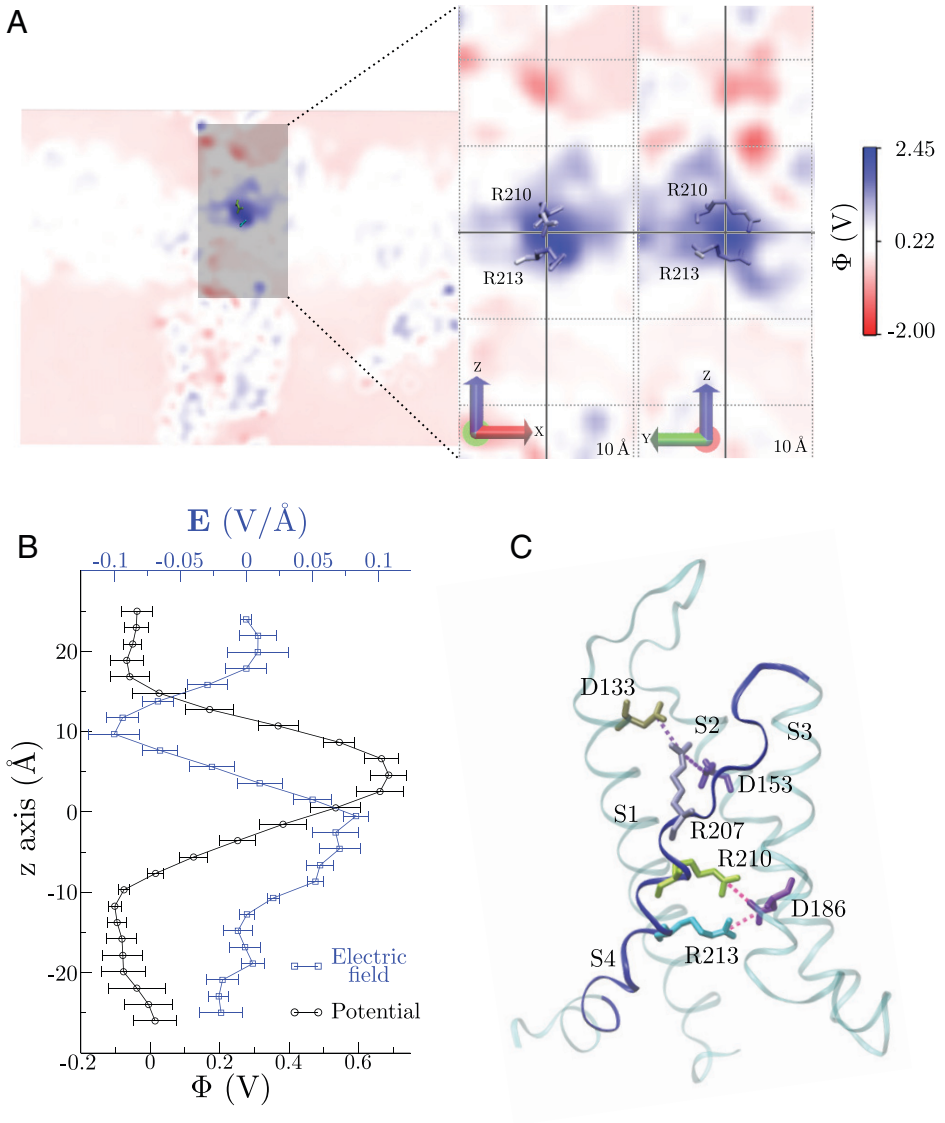

Fig. 4. The membrane electric field is focused on the VSD dry zone. (*A*) VSD electrostatic potential profiles (Φ) in the R210-R213 plane (*Left*). A closer view of Φ shows the membrane electric field is highly focused on the gating charges populating the VSD dry zone. (*B*) Average Φ (over time and for the four monomers) and electric field along the *z* axis; Φ was computed within a 10-Å radius cylinder along z −25 Å < z < 25 Å. (*C*) VSD salt bridges observed during the 0.5-μs simulation. *Top*: average distances over time and for the four monomers between arginines and aspartates. *Bottom*: graphical depiction of each salt bridge with the VSD represented as cyan transparent cartoon. Error bars represent the SD of the time average for the four monomers.

movement of R213 mirrored that of R210, albeit with a smaller upward displacement of 2 Å (Fig. 5*B* and *SI Appendix*, Fig. S4 *A* and *B*, *Bottom*). Note that, unlike the replica shown in Fig. 5*A*, in the replicas depicted in *SI Appendix*, Fig. S4 *A* and *B*, we observed nonreactive VSDs during the whole simulation (*SI Appendix*, Fig. S4; red and black traces). At rest (0 mV), R210 was the only charge positioned between the two isopotential extra and intracellular solutions and interacted with the π face of F160 in S1 and with D186 in S3 (Fig. 5*C*). A more detailed view of the interactions of R210 at rest with other residues in the VSD shows that this gating charge was also near V185 in S3, creating a hydrophobic environment that surrounded R210 (*SI Appendix*, Fig. S2 *A* and *C*). However, at positive voltages (active state), R210 suffered an upward displacement, approaching the hydrated external region of the VSD (Fig. 5*D*). On the other hand, upon activation, R213 underwent an upward movement, and its new position virtually overlapped with the position previously occupied by R210 at the resting state (Fig. 5*D* and *SI Appendix*, Fig. S2 *B* and *D*).

F160 and V185 appeared to define the boundaries of the dry zone, where R210 and R213 moved in response to the membrane electric field. This way, the number of water molecules around R210 was reduced at rest, where R210 interacted with F160 and V185. In the active state, however, R210 moved upward to a more hydrated region, while R213 dehydrated by moving into the dry zone (Fig. 2 *B* and *D*). These results are highly consistent with the neutralization scanning (Fig. 1) discussed in the previous sections and point to an activation model wherein minimal displacement of S4 can explain the VSD's charge movement and activation process. In particular, the larger displacement of R210 compared to that of R213 in our MD simulations is consistent with the observation that R210 displaced about 66% of the total gating charge. Under these conditions, z_Q was reduced from 0.62 ± 0.02 e_0 in the wt to 0.27 ± 0.02 e_0 in the R210Q neutralization mutant (*SI Appendix*, Table S1).

VSD Resting/Active Equilibrium Is Set by Electrostatic Interactions. As is the case in most VSDs (43), our simulations show that the charged residues within the VSD formed a dynamic

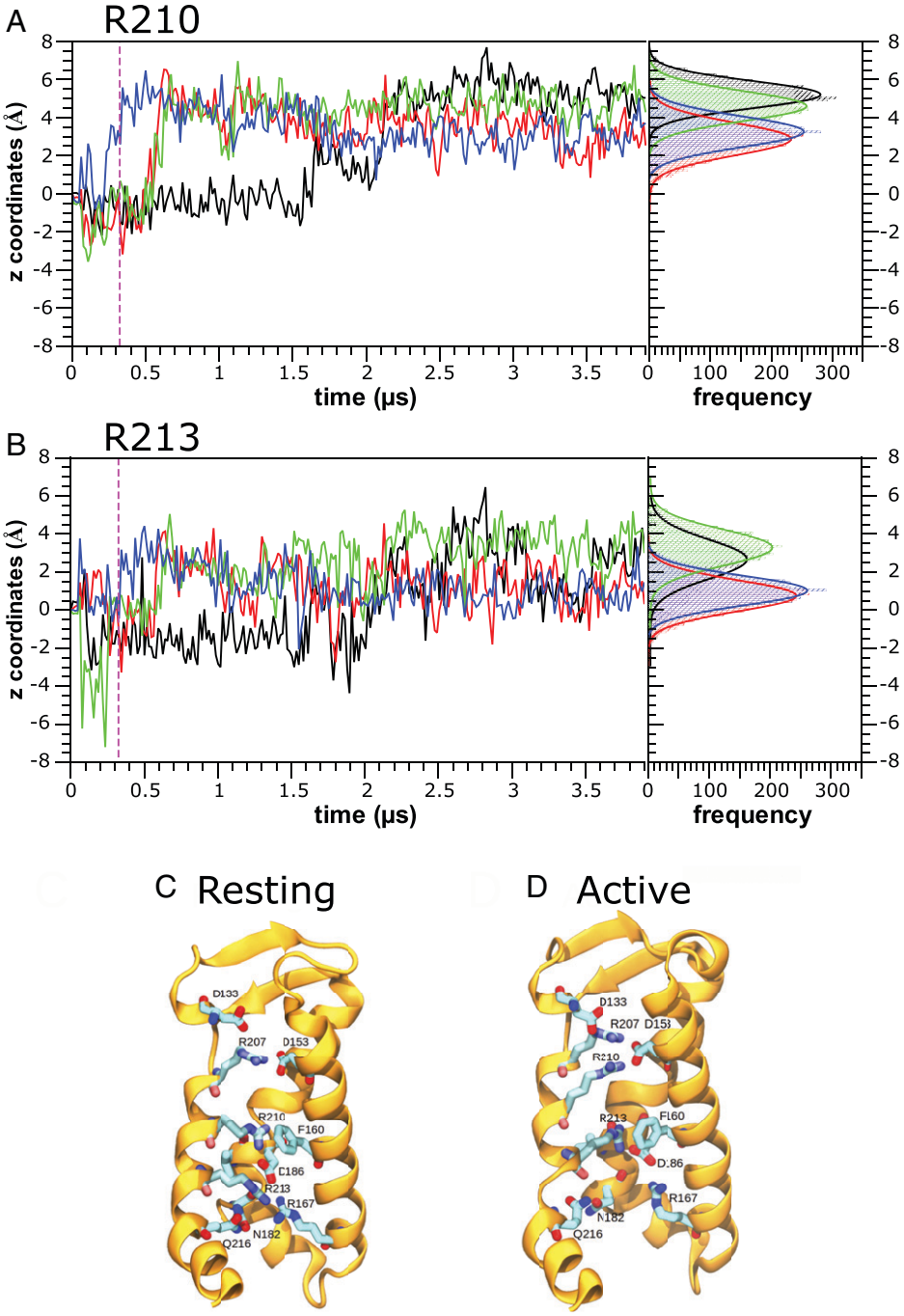

Fig. 5. Molecular simulations in the presence of electric field shows an upward displacement of the BK gating charges. (*A* and *B*) *z* Axis displacement of the guanidine group CZ atom as a function of time for (*A*) Arginine 210 and (*B*) Arginine 213. Events are plotted for the entire ~3.9-μs MD simulations under an external electric field (+400 mV). Each color represents the arginine from an individual sensor of the BK channel, and an all-points histogram of the last 500 ns is shown to the right of each panel for better visualization of the final position of the gating charge. The plot shows that both R210 and R213 tend to raise their position in each sensor about 4 Å in the case of R210 and 2 Å in the case of R213. Vertical magenta dashed lines indicate the moment in which the electric field began to be applied during the simulation. (*C*) BK VSD in the resting state obtained from a simulation under equilibrium in the absence of electric field. R207 is interacting with D153, while both R210 and R213 are in contact with D186. (*D*) BK VSD in the active state obtained after 3 μs of MD simulation under an external electric field (+400 mV). R210 and R213 move up; thus, R210 now appears to be interacting with D153, while R213 makes interactions with F160 and D186.

salt-bridge network. To generate a molecular picture of the electrostatic landscape determining this VSD $A-R$ equilibrium, we performed 500-ns MD simulations of the transmembrane domain of the R207Q and D153N mutants at zero electric field conditions, whose $Q(V)$ relations were largely biased toward the active and resting states, respectively. In line with our experimental results, within the VSD of the R207Q mutant, R210 experienced an upward movement (Fig. 6 *A* and *C*, *Bottom*) that resembles the active state of the wt channel model obtained in the presence of a depolarizing potential (Fig. 5*A*). On the other hand, and consistent with a resting state stabilization, the D153N mutant did not exhibit major displacements of the R210-213 pair (Fig. 6 *B* and *C*, *Top*). The electrostatic hypothesis gets additional support after computing the electrostatic energy difference of VSD activation associated with the charge neutralization, calculated via Coulomb's law, based only on the displacements of R210 and R213 observed in Fig. 5 *A* and *B*. Specifically, the electrostatic energy difference of VSD activation associated with the charge neutralization ($\Delta\Delta U_E$) was calculated using the following equation:

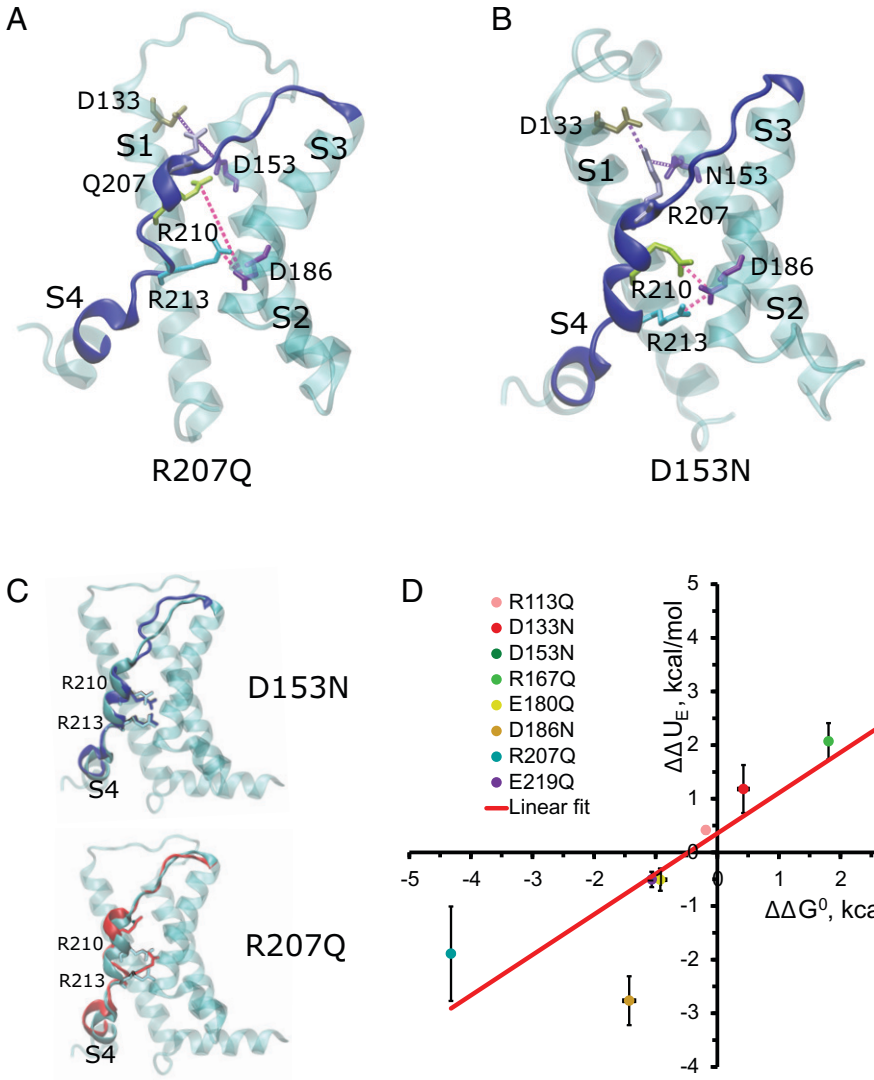

Fig. 6. The VSD resting/active equilibrium is set by electrostatic interactions. (*A* and *B*) Representative frame extracted from a 500-ns molecular simulation of the mutants (*A*) R207Q and (*B*) D153N. BK channel mutants show a salt-bridge network that tunes the R-A VSD equilibrium. Magenta and purple lines represent salt bridges betwen corresponding amino acids. (*C*) Overlap of the VSD of the BK wt channel (cyan, Fig. 2*B*) and the S4 segment (red) of the BK R207Q mutant channel (*Bottom*) and S4 of the D153N (blue; *Top*). (*D*) Correlation between electrostatic energy differences of VSD activation associated with the charge neutralization ($\Delta\Delta U_E$;Eq. **4**) and $\Delta(\Delta G^0)$ obtained from the shift along the voltage axis of each neutralization mutant (*SI Appendix*, Table S1). Error bars = SD.

$$\Delta\Delta U_E = -332\frac{z_1 z_2}{\varepsilon}\left(\frac{1}{r_{12}^*} - \frac{1}{r_{12}}\right) \qquad [4]$$

where the constant 332 represents a conversion factor in kcal/mol, with $z_1 = 2$, the charge of the arginines 210 and 213 expressed in times the elementary charge; z_2 is the charge of the neutralized residues, either 1 or -1; ε is the dielectric constant; and r_{12} and r_{12}^* are the distances, measured in Å, from the charge of the mutated residue and those of the center of mass of R210 and R213 guanidinium moieties in the resting and activated state, respectively. As shown in Fig. 6*D*, the $\Delta\Delta U_E$ correlates well with the $\Delta(\Delta G^0)$ obtained from the shift along the voltage axis of each neutralization mutant, thus being consistent with the electrostatic hypothesis that explains the above-mentioned $Q(V)$ curve shifts.

Several Charged Residues in the BK VSD Participate in the Allosteric Modulation of the PD by Voltage. To get a better description of the effect of VSD neutralization mutants on VSD activation energetics, we fitted the normalized tail current-voltage data (*SI Appendix*, Fig. S3) using an equation for the open probability (P_o) derived from a model that assumes a central closed-open transition modulated allosterically by the four voltage sensors (21):

$$P_o = \frac{1}{1 + \frac{(1+J)^4}{L(1+DJ)^4}} \qquad [5]$$

where $L = L_0 e^{z_L FV/RT}$ is the equilibrium constant of the closed-open transition in the absence of Ca^{2+} and all voltage sensors at rest; z_L is the number of elementary charges associated with the opening transition, L_0 is the value of L at $V = 0$, and D is the allosteric factor describing the strength of the interaction between channel opening and VSD activation. Our gating current measurements provide the values of V_0 and z_J necessary to calculate J (Eq. **1**). Since all mutations are in the VSD, we assumed that the parameters L_0 and z_L that define the closed-open transition remained unaltered in the mutants. Fitting of the normalized tail currents (*SI Appendix, Materials and Methods*) was performed using the values for L_0 and z_L reported in Ma et al. (2006) (33), while we allowed the allosteric coupling between the VSD and the pore (D) to vary. All

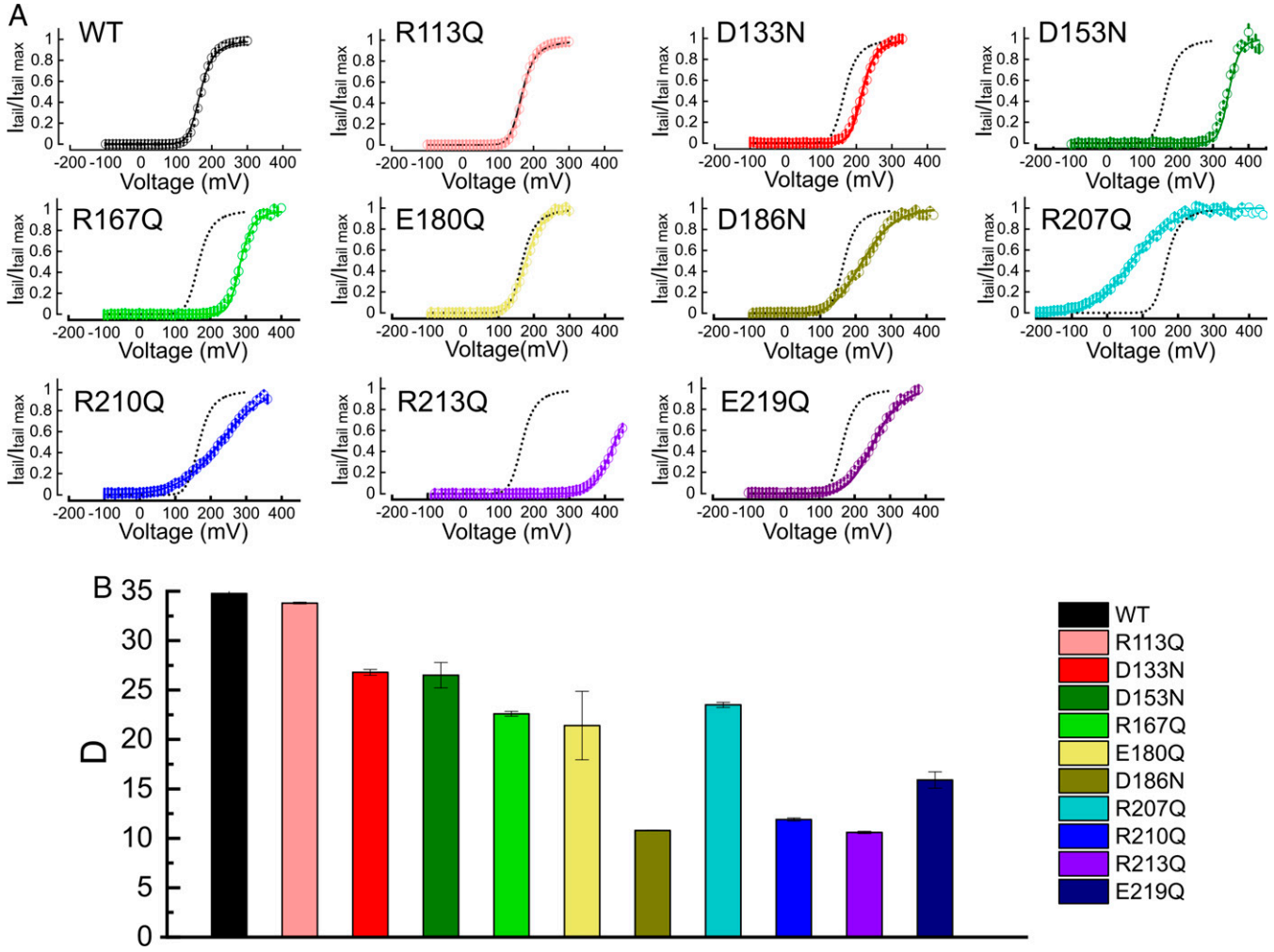

Fig. 7. Neutralization mutants decrease the VSD-PD allosteric coupling. (*A*) Normalized tail current amplitude ($I_{tail}/I_{tail,max}$) versus voltage relation for BK wt and the VSD neutralization variants. Colored solid lines represent the best fit to the H-A allosteric model, where J_0 and z_J were obtained from experiments shown in Fig. 1 and L_0 and z_L remained constant for all channels except for D186N, R207Q, and R210Q, where z_L could vary to fit the experimental data. All parameter fitting is reported in *SI Appendix*, Table S2. (*B*) Allosteric coupling constant ±S.E. (*D*) between the VSD and the PD obtained from the fittings of the $I_{tail}/I_{tail,max}$ data using Eq. **5**.

mutants, except for D186N, R210Q, and R213Q, were fitted reasonably well by decreasing D between ∼10 and 50% (Fig. 7 *A* and *B* and *SI Appendix*, Table S2), suggesting that the electrostatic network influencing the VSD $A-R$ equilibrium also sets their energetic crosstalk with the PD.

Mutants R210Q and R213Q showed the most dramatic decrease in D, with values of 11.9 ± 0.16 and 10.6 ± 0.12, respectively. Interestingly, due to their very negative V_0, mutants D186N, R207Q, and R210Q had most of their voltage sensors in the active state at voltages at which P_O was very low (Figs. 1*C* and 7*A*); therefore, Eq. **5** can be approximated to (21)

$$P_o \approx \frac{1}{1+\frac{1}{L(D)^4}} \qquad [6]$$

Eq. **6** predicts that the voltage dependence of the conductance-voltage curves should match the voltage dependence of the pore opening z_L reported for wt BK channels [$z_L = 0.3$ (33)]. Fitting the curves for D186N, R207Q, and R210Q to Eq. **5** required leaving z_L as a free parameter; the best fit was obtained for z_L equal to 0.49 ± 0.01, 0.42 ± 0.01, and 0.43 ± 0.01, respectively (*SI Appendix*, Table S2). Considering that these values are close to the z_L for wt channels, it seems plausible that these charge neutralizations mainly decrease the strength of coupling between VSDs and the PD without affecting the intrinsic voltage dependency of the pore opening. Overall, these results suggest that i) the electrostatic tuning of the VSD $A-R$ equilibrium also modulates the allosteric coupling energetics and ii) R210 and R213, in addition to their role as gating charge carriers in BK channels, also modulate the VSD-PD allosteric coupling.

Discussion

Although three of the Kv channels' S4 voltage-sensing arginines are conserved in BK (R207, R210, and R213 in the human BK) (24) (Fig. 1*A*), the voltage dependence of the BK $Q(V)$ curve is known to be much shallower than that of Kv channels (21, 32). Consistently, the total number of gating charges per channel ($4z_Q$) calculated from the slope of the $Q(V)$ is about 2.4 e_0 (21, 32, 38–40, 44, 45), a notable reduction compared with the 12 to 13 e_0 reported for other voltage-activated K^+ channels (46, 47). This observation raises questions regarding the identity and equivalence of the BK and Kv channel gating charges, as well as the mechanism by which they sense and respond to changes in membrane potential.

Identification of the BK gating charges has been hindered by the limited coupling between VSD activation and pore opening,

which impedes the use of classical methods such as the limiting slope determination (21, 48, 49). In BK channels, the limiting slope strictly reflects the voltage dependence of pore opening. By analyzing the voltage dependence of the conductance-voltage curves ($G(V)$) at different Ca^{2+} concentrations and interpreting their results using the Horrigan and Aldrich allosteric model (H-A model), Ma et al. (2006) (33) concluded that the residues involved in voltage sensing likely spread over S2 (D153 and R167), S3 (D186), and S4 (R213). Here, we were able to circumvent the uncertainties of model fitting by assessing the effects of neutralizing each of the charged residues spanning S1 to S4 on BK channel gating by direct estimates based on the VSD charge displacement. Of the four gating charges predicted by Ma et al. (33), we only confirmed R213; our experimental determination of the z_J of this mutant was virtually identical to that predicted by them. Contrary to their findings, however, we also detected a reduction of about 50% in z_J after neutralization of R210. These results unambiguously identify R210 and R213 as the likely BK gating charges. In doing so, we can discount all remaining residues in S1 to S4 as putative charge carriers. Importantly, histidine replacement of R210 in the presence of a pH gradient led to an inward rectifier proton channel, suggesting that gating charge movements must occur within a very narrow septum rather than moving between two hydrated vestibules through a gating charge transfer center, as reported for Kv channels (36). This mechanism is fully consistent with MD simulations of the resting state of the BK VSD [based on h*Slo* (35); Fig. 5], showing that two aqueous vestibules appear to be separated by a septum containing residues R210 and R213. Application of an electric field led to side chain reorientations toward the extracellular face of the sensor, wherein R210 became solvent-exposed in the VSD active state. Our results are in agreement with the accessibility experiments of Hu et al. (2003) (50) showing that at 80 mV a cysteine in position 210 (R210C mutant) was exposed to the external solution, whereas R213 could only be modified from the internal side of the membrane. At −80 mV, the BK voltage sensor of the R210C mutant was in the active configuration, indicating that a cysteine in position 210 would be exposed to the external solution at that voltage (*SI Appendix*, Table S1).

While the $Q(V)$ relationship for BK wt has been reproduced by several groups, our results with the VSD neutralization variants depart from some of the parameters reported by Ma et al. (2006) (33) using the H-A model. While Ma et al. estimated that z_J decreases by half after neutralization of D186, this study found little or no change in D186N z_J, yet V_0 was left-shifted by ∼100 mV (Fig. 1 *C* and *D* and *SI Appendix*, Table S1). Thus, the coupling between voltage sensor activation and pore opening appears compromised in this mutant (Fig. 7*B* and *SI Appendix*, Table S2). Neutralizing D153 decreased the electronegativity along the extracellular face of the VSD, imposing an electrostatic bias to the field sensed by R210 and R213, stabilizing the voltage sensor in its resting conformation ($\Delta V_0 = 168$ mV). This is consistent with the observation that negatively charged residues at the extracellular face of the VSD might be involved in BK inhibition caused by low pH (51). Both residues D133 and D153 in h*Slo* (35) appear to make salt bridges with R207 (4.7 ± 0.2Å and 4.0 ± 0.2Å, respectively). However, while D133 is exposed to the external solution, D153 is completely embedded in the VSD. This indicates that the charged D133 can be electrostatically screened by the external medium, whereas D153, with a longer Debye length, likely exerts a stronger effect on the resting–active equilibrium of the VSD. In the case of the R207Q mutant, our estimation of z_J and J_0 is in agreement with published values (33).

Zhang et al. (2014) (52) reported that the mutation E219R left-shifted the $Q(V)$ by −126 mV, increasing the number of apparent gating charges per voltage sensor from 0.5 in the wt to 0.66. Our data show that E219Q is left shifted −51 mV with essentially no change in z_Q (*SI Appendix*, Table S1). These results are consistent with the electrostatic hypothesis that either the neutralization E219Q mutant or the reverse charge E219R mutant introduces electrostatic biases destabilizing the resting conformation of the voltage sensor. As expected, the shift induced by the E219R mutant is larger than that of E219Q and scales according to its positive electrostatic potential in the neighborhood of R213. We note that those mutations that promote shifts to the $Q(V)$ curve V_h also show corresponding shifts in Förster resonance energy transfer efficiency versus voltage curves (53). This also points to the existence of an interaction between the voltage sensor and the gating ring, which would be essential for determining the set point of the voltage sensor equilibrium (39) under physiological conditions.

Here, we propose a voltage-sensing mechanism for BK channels that diverges from that found in Kv channels and voltage-dependent enzymes, where the charges move between two aqueous vestibules separated by a hydrophobic plug with significant movement of S4 (54, 55). Instead, we suggest a mechanism where guanidinium moieties in BK residues R210 and R213—the VSD gating charges—experience small rotameric displacements across a focused membrane electric field dry zone. In this proposal, BK gating charges are equivalent to R365 and R368 from Shaker channels. Unlike Kv channels, however, none of them move far enough to access both aqueous vestibules during VSD activation. These observations explain why displacement of both R210 and R213 together in BK is equivalent to about 0.6 e_0, while movement of R365 and R368 residues in Shaker contribute ∼1 e_0 each to the effective valence (46). Our h*Slo*-based (35) MD simulations show a dry zone of about the same thickness as that of the septum that catalyzes the gating charge transfer in Kv channels (54, 56). However, unlike Kv channels, in BK the S4 α helix undergoes very small movement during voltage activation [see also Hite et al., 2017 (23)].

These contrasting observations point to different voltage-sensing mechanisms in Kv and BK channels: While the former focuses its electric field in a thin hydrophobic gap, thus allowing the rapid passage of four of the S4 positively charges, in the latter this dry zone is thicker (∼10 Å). Thus, a thicker dry zone favors the long-range electrostatic tuning of VSD $A-R$ transition by decreasing the dielectric constant around the gating charges. It is worth mentioning here that in the case of the *Ciona intestinalis* VSD (CiVSD) activation, S4 undergoes a rotation and a 5-Å upward displacement (8), where the site occupied by R2 and R3 in the resting CiVSD is occupied by R3 and R4 in the active CiVSD conformation, transferring about 1 e_0. Just as suggested here, these changes are accompanied by rotameric reorientations of arginine guanidinium groups. Importantly, even though the CiVSD displaces an amount of charge in the same range as that of the BK channel VSD (∼1 e_0), gating current kinetics in BK are about 1,000-fold faster than that of CiVSD. Our results give a parsimonious explanation for this large difference in activation kinetics, where overall gating-charge transfer in BK VSD mostly depends on the rotameric reorientation of the arginines and can be achieved through small changes in global S4 conformation. In light of the present results and given that in BK the VSD and PD are in a nonswapped configuration, we suggest that the coupling between the VSD and the PD cannot take place through a "classical" Kv channel electromechanical coupling (57–59).

Thus, it seems plausible that the tight antiparallel packing between S4 and S5 (24) couples the small displacement of S4 to the changes in S6 necessary to change the internal vestibule diameter so as to produce the hydrophobic gating induced by Ca^{2+}, as suggested by the Cui group (60). The issue of how a small conformational change in the VSD has such a high impact in the open probability of the pore is intriguing and is still a matter of intense debate and research.

Materials and Methods

Homology models of BK channels were made from human Slo1 channels (35), and MD simulations were done with NAMDv2.14 using the CHARMM36 force field. The electrophysiological experiments were performed by clamping macropatches on *Xenopus laevis* oocytes. Ionic currents were recorded in the presence of symmetrical 110 mM K^+, and gating currents were recorded in the absence of permeant ions. Detailed materials and methods are included in *SI Appendix*.

Data Availability. All study data are included in the article and/or *SI Appendix*.

ACKNOWLEDGMENTS. We thank Mrs. Luisa Soto (Universidad de Valparaiso) for excellent technical assistance and Drs. Francisco Bezanilla and John Ewer for their careful reading of the manuscript. This research was supported by the Fondo Nacional de Desarrollo Científico y Tecnológico (FONDECYT) Regular Grant Nos. 1190203 (to R.L.), 1170733 (to F.D.G.-N.), 1221260 (to J.A.G.), and FONDECYT Postdoctorado 3170599 (to I.D.-F.), Proyecto PAI7719087 (to I.D.-F.); US Army Research Office Cooperative Agreement W911NF-17-2-0081 (to F.D.G.N.); a US Air Force Office of Scientific Research grant under award FA9550-16-1-0384 (to R.L.); and NIH Grant No. GM030376 (to R.L.). The Centro Interdisciplinario de Neurociencias de Valparaiso (CINV) and Millenium Nucleus in NanoBioPhysics (NNBP) are supported by the Iniciativa Científica Milenio-Agencia Nacional de Investigación y Desarrollo (ICM-ANID), Project P09-022-F (CINV), and Project NCN2021, NNBP (to J.A.G). The Centro Ciencia & Vida is supported by the Financiamiento Basal para Centros Científicos y Tecnológicos de Excelencia de ANID Project FB210008 (to J.A.G).

Author affiliations: [a]Centro Interdisciplinario de Neurociencia de Valparaíso, Facultad de Ciencias, Universidad de Valparaíso, Valparaíso 2340000, Chile; [b]Center for Bioinformatics and Integrative Biology, Facultad de Ciencias de la Vida, Universidad Andrés Bello, Santiago 8370146, Chile; [c]Millennium Nucleus in NanoBioPhysics, Valparaíso 2340000, Chile; [d]Centro Científico y Tecnológico de Excelencia Ciencia & Vida, Santiago 7810000, Chile; [e]Department of Biochemistry and Molecular Biology, The University of Chicago, Chicago, IL 60637; [f]Grossman Institute for Neuroscience, Quantitative Biology and Human Behavior, The University of Chicago, Chicago, IL 60637; [g]Departamento de Biología, Facultad de Ciencias, Universidad de Chile, Santiago 7810000, Chile; and [h]Centro de Nanotecnología Aplicada, Facultad de Ciencias, Universidad Mayor, Santiago, Chile, 8580745

1. J. S. Trimmer, K. J. Rhodes, Localization of voltage-gated ion channels in mammalian brain. *Annu. Rev. Physiol.* **66**, 477–519 (2004).
2. H. Vacher, D. P. Mohapatra, J. S. Trimmer, Localization and targeting of voltage-dependent ion channels in mammalian central neurons. *Physiol. Rev.* **88**, 1407–1447 (2008).
3. E. Balse *et al.*, Dynamic of ion channel expression at the plasma membrane of cardiomyocytes. *Physiol. Rev.* **92**, 1317–1358 (2012).
4. M. N. Foster, W. A. Coetzee, KATP channels in the cardiovascular system. *Physiol. Rev.* **96**, 177–252 (2016).
5. N. Schmitt, M. Grunnet, S. P. Olesen, Cardiac potassium channel subtypes: New roles in repolarization and arrhythmia. *Physiol. Rev.* **94**, 609–653 (2014).
6. F. H. Yu, W. A. Catterall, The VGL-chanome: A protein superfamily specialized for electrical signaling and ionic homeostasis. *Sci. STKE* **2004**, re15 (2004).
7. É. Faure, G. Starek, H. McGuire, S. Bernèche, R. Blunck, A limited 4 Å radial displacement of the S4-S5 linker is sufficient for internal gate closing in Kv channels. *J. Biol. Chem.* **287**, 40091–40098 (2012).
8. Q. Li *et al.*, Structural mechanism of voltage-dependent gating in an isolated voltage-sensing domain. *Nat. Struct. Mol. Biol.* **21**, 244–252 (2014).
9. Q. Li, S. Wanderling, P. Sompornpisut, E. Perozo, Structural basis of lipid-driven conformational transitions in the KvAP voltage-sensing domain. *Nat. Struct. Mol. Biol.* **21**, 160–166 (2014).
10. E. Vargas *et al.*, An emerging consensus on voltage-dependent gating from computational modeling and molecular dynamics simulations. *J. Gen. Physiol.* **140**, 587–594 (2012).
11. V. Yarov-Yarovoy *et al.*, Structural basis for gating charge movement in the voltage sensor of a sodium channel. *Proc. Natl. Acad. Sci. U.S.A.* **109**, E93–E102 (2012).
12. G. Dai, T. K. Aman, F. DiMaio, W. N. Zagotta, The HCN channel voltage sensor undergoes a large downward motion during hyperpolarization. *Nat. Struct. Mol. Biol.* **26**, 686–694 (2019).
13. M. A. Kasimova *et al.*, Helix breaking transition in the S4 of HCN channel is critical for hyperpolarization-dependent gating. *eLife* **8**, e53400 (2019).
14. C. H. Lee, R. MacKinnon, Voltage sensor movements during hyperpolarization in the HCN channel. *Cell* **179**, 1582–1589.e1587 (2019).
15. H. G. Knaus *et al.*, Distribution of high-conductance Ca(2+)-activated K+ channels in rat brain: Targeting to axons and nerve terminals. *J. Neurosci.* **16**, 955–963 (1996).
16. A. N. Poulsen *et al.*, Differential expression of BK channel isoforms and beta-subunits in rat neurovascular tissues. *Biochim. Biophys. Acta* **1788**, 380–389 (2009).
17. S. I. Dworetzky, J. T. Trojnacki, V. K. Gribkoff, Cloning and expression of a human large-conductance calcium-activated potassium channel. *Brain Res. Mol. Brain Res.* **27**, 189–193 (1994).
18. L. Chen *et al.*, Membrane trafficking of large conductance calcium-activated potassium channels is regulated by alternative splicing of a transplantable, acidic trafficking motif in the RCK1-RCK2 linker. *J. Biol. Chem.* **285**, 23265–23275 (2010).
19. R. Latorre *et al.*, Molecular determinants of BK channel functional diversity and functioning. *Physiol. Rev.* **97**, 39–87 (2017).
20. C. S. Bailey, H. J. Moldenhauer, S. M. Park, S. Keros, A. L. Meredith, KCNMA1-linked channelopathy. *J. Gen. Physiol.* **151**, 1173–1189 (2019).
21. F. T. Horrigan, R. W. Aldrich, Coupling between voltage sensor activation, Ca^{2+} binding and channel opening in large conductance (BK) potassium channels. *J. Gen. Physiol.* **120**, 267–305 (2002).
22. J. Cui, D. H. Cox, R. W. Aldrich, Intrinsic voltage dependence and Ca^{2+} regulation of mslo large conductance Ca-activated K^+ channels. *J. Gen. Physiol.* **109**, 647–673 (1997).
23. R. K. Hite, X. Tao, R. MacKinnon, Structural basis for gating the high-conductance Ca^{2+}-activated K^+ channel. *Nature* **541**, 52–57 (2017).
24. X. Tao, R. K. Hite, R. MacKinnon, Cryo-EM structure of the open high-conductance Ca^{2+}-activated K^+ channel. *Nature* **541**, 46–51 (2017).
25. C. H. Lee, R. MacKinnon, Structures of the human HCN1 hyperpolarization-activated channel. *Cell* **168**, 111 (2017).
26. J. R. Whicher, R. MacKinnon, Structure of the voltage-gated K^+ channel Eag1 reveals an alternative voltage sensing mechanism. *Science* **353**, 664–669 (2016).
27. A. L. Blatz, K. L. Magleby, Ion conductance and selectivity of single calcium-activated potassium channels in cultured rat muscle. *J. Gen. Physiol.* **84**, 1–23 (1984).
28. B. S. Pallotta, Single channel recordings from calcium-activated potassium channels in cultured rat muscle. *Cell Calcium* **4**, 359–370 (1983).
29. R. Latorre, C. Vergara, C. Hidalgo, Reconstitution in planar lipid bilayers of a Ca2+-dependent K+ channel from transverse tubule membranes isolated from rabbit skeletal muscle. *Proc. Natl. Acad. Sci. U.S.A.* **79**, 805–809 (1982).
30. A. Marty, Ca-dependent K channels with large unitary conductance in chromaffin cell membranes. *Nature* **291**, 497–500 (1981).
31. M. Wallner, P. Meera, L. Toro, Determinant for beta-subunit regulation in high-conductance voltage-activated and Ca^{2+}-sensitive K^+ channels: An additional transmembrane region at the N terminus. *Proc. Natl. Acad. Sci. U.S.A.* **93**, 14922–14927 (1996).
32. E. Stefani *et al.*, Voltage-controlled gating in a large conductance Ca^{2+}-sensitive K^+channel (hslo). *Proc. Natl. Acad. Sci. U.S.A.* **94**, 5427–5431 (1997).
33. Z. Ma, X. J. Lou, F. T. Horrigan, Role of charged residues in the S1-S4 voltage sensor of BK channels. *J. Gen. Physiol.* **127**, 309–328 (2006).
34. L. Díaz *et al.*, Role of the S4 segment in a voltage-dependent calcium-sensitive potassium (hSlo) channel. *J. Biol. Chem.* **273**, 32430–32436 (1998).
35. X. Tao, R. MacKinnon, Molecular structures of the human Slo1 K^+ channel in complex with β4. *eLife* **8**, e51409 (2019).
36. X. Tao, A. Lee, W. Limapichat, D. A. Dougherty, R. MacKinnon, A gating charge transfer center in voltage sensors. *Science* **328**, 67–73 (2010).
37. M. C. Lin, J. Y. Hsieh, A. F. Mock, D. M. Papazian, R1 in the Shaker S4 occupies the gating charge transfer center in the resting state. *J. Gen. Physiol.* **138**, 155–163 (2011).
38. G. F. Contreras, A. Neely, O. Alvarez, C. Gonzalez, R. Latorre, Modulation of BK channel voltage gating by different auxiliary β subunits. *Proc. Natl. Acad. Sci. U.S.A.* **109**, 18991–18996 (2012).
39. Y. Lorenzo-Ceballos, W. Carrasquel-Ursulaez, K. Castillo, O. Alvarez, R. Latorre, Calcium-driven regulation of voltage-sensing domains in BK channels. *eLife* **8**, e44934 (2019).
40. W. Carrasquel-Ursulaez *et al.*, Hydrophobic interaction between contiguous residues in the S6 transmembrane segment acts as a stimuli integration node in the BK channel. *J. Gen. Physiol.* **145**, 61–74 (2015).
41. D. M. Starace, F. Bezanilla, Histidine scanning mutagenesis of basic residues of the S4 segment of the shaker K^+ channel. *J. Gen. Physiol.* **117**, 469–490 (2001).
42. D. M. Starace, F. Bezanilla, A proton pore in a potassium channel voltage sensor reveals a focused electric field. *Nature* **427**, 548–553 (2004).
43. J. R. Groome, L. Bayless-Edwards, Roles for countercharge in the voltage sensor domain of ion channels. *Front. Pharmacol.* **11**, 160 (2020).
44. L. Bao, D. H. Cox, Gating and ionic currents reveal how the BK_{Ca} channel's Ca^{2+} sensitivity is enhanced by its β1 subunit. *J. Gen. Physiol.* **126**, 393–412 (2005).
45. F. T. Horrigan, R. W. Aldrich, Allosteric voltage gating of potassium channels II. Mslo channel gating charge movement in the absence of Ca^{2+}. *J. Gen. Physiol.* **114**, 305–336 (1999).
46. S. A. Seoh, D. Sigg, D. M. Papazian, F. Bezanilla, Voltage-sensing residues in the S2 and S4 segments of the Shaker K+ channel. *Neuron* **16**, 1159–1167 (1996).
47. S. K. Aggarwal, R. MacKinnon, Contribution of the S4 segment to gating charge in the Shaker K^+ channel. *Neuron* **16**, 1169–1177 (1996).
48. D. Sigg, F. Bezanilla, Total charge movement per channel. The relation between gating charge displacement and the voltage sensitivity of activation. *J. Gen. Physiol.* **109**, 27–39 (1997).
49. W. Almers, Gating currents and charge movements in excitable membranes. *Rev. Physiol. Biochem. Pharmacol.* **82**, 96–190 (1978).
50. L. Hu *et al.*, Participation of the S4 voltage sensor in the Mg^{2+}-dependent activation of large conductance (BK) K^+ channels. *Proc. Natl. Acad. Sci. U.S.A.* **100**, 10488–10493 (2003).
51. Y. Zhou, X. M. Xia, C. J. Lingle, BK channel inhibition by strong extracellular acidification. *eLife* **7**, e38060 (2018).

52. G. Zhang *et al.*, A charged residue in S4 regulates coupling among the activation gate, voltage, and Ca^{2+} sensors in BK channels. *J. Neurosci.* **34**, 12280–12288 (2014).
53. P. Miranda, M. Holmgren, T. Giraldez, Voltage-dependent dynamics of the BK channel cytosolic gating ring are coupled to the membrane-embedded voltage sensor. *eLife* **7**, e40664 (2018).
54. J. J. Lacroix, H. C. Hyde, F. V. Campos, F. Bezanilla, Moving gating charges through the gating pore in a Kv channel voltage sensor. *Proc. Natl. Acad. Sci. U.S.A.* **111**, E1950–E1959 (2014).
55. L. D. Islas, F. J. Sigworth, Electrostatics and the gating pore of Shaker potassium channels. *J. Gen. Physiol.* **117**, 69–89 (2001).
56. V. Jogini, B. Roux, Dynamics of the Kv1.2 voltage-gated K^+ channel in a membrane environment. *Biophys. J.* **93**, 3070–3082 (2007).
57. S. B. Long, E. B. Campbell, R. Mackinnon, Crystal structure of a mammalian voltage-dependent Shaker family K^+ channel. *Science* **309**, 897–903 (2005).
58. Z. Batulan, G. A. Haddad, R. Blunck, An intersubunit interaction between S4-S5 linker and S6 is responsible for the slow off-gating component in Shaker K^+ channels. *J. Biol. Chem.* **285**, 14005–14019 (2010).
59. Z. Lu, A. M. Klem, Y. Ramu, Coupling between voltage sensors and activation gate in voltage-gated K^+ channels. *J. Gen. Physiol.* **120**, 663–676 (2002).
60. Z. Jia, M. Yazdani, G. Zhang, J. Cui, J. Chen, Hydrophobic gating in BK channels. *Nat. Commun.* **9**, 3408 (2018).